Acta Crystallographica Section B
Structural Science
ISSN 0108-7681

Symmetry of platelet defects in diamond: new insights with synchrotron light

Alexei Bosak,[a] Dmitry Chernyshov,[b]* M. Krisch[a] and Leonid Dubrovinsky[c]

[a]European Synchrotron Radiation Facility, BP 220, 38043 Grenoble CEDEX, France, [b]Swiss–Norwegian Beam Lines, BP 220, 38043 Grenoble CEDEX, France, and [c]Bayerisches Geoinstitut, Universität Bayreuth, D-95440 Bayreuth, Germany

Correspondence e-mail: dmitry.chernyshov@esrf.fr

Received 2 March 2010
Accepted 3 August 2010

Mapping of reciprocal space for *Ia*-type diamond single crystals with synchrotron radiation has uncovered a variety of diffuse scattering features, some of them have not been observed before. The main component of diffuse scattering in the form of diffuse rods corresponds to a set of platelets which join together blocks of diamond structure. The platelets are ordered structural entities with lattice periodicity $8^{1/2}a_0 \times (1/2)^{1/2}a_0 \times 0.55a_0$, where a_0 is a unit-cell dimension of diamond. Intensity distribution along the rods has been measured and used for recognition of symmetry elements of the platelet structure. These findings, together with previously reported transmission electron microscopy (TEM) observations, provide strong constraints for atomistic modelling of the platelet structure.

1. Introduction

Diamond is commonly considered as one of the hardest materials having very ordered arrangements of atoms. However, the majority of diamonds, natural or synthetic, contain a variety of defects, ranging from substitutional impurities to micrometer-sized defect aggregates. Most of the defects affect the physical properties of diamonds and can be crucial for the applications (Neves & Nazaré, 2001; Zaitsev, 2001; Davies *et al.*, 2004; Webb & Jackson, 1995).

The small atomic radius of C atoms and their strong covalent bonds make incorporation of other elements in diamond structure very difficult. Nitrogen is a notable exception from this rule – its concentration can be as high as 0.3%. Nitrogen forms a variety of defects, giving rise to characteristic bands in the optical absorption spectra (Zaitsev, 2001) and this fact is widely used for classification of diamonds based on their IR spectra. Diamonds with a predominance of single substitutional atoms (C defects) – the absolute majority of synthetic diamonds grown under high pressure/high temperature conditions – are called *Ib*-type. Among natural diamonds aggregates of defects are much more typical; nitrogen aggregation is described by the sequence $C \Rightarrow A \Rightarrow B$, where A denotes a pair of neighboring substitutional N atoms and B four N atoms around a vacancy. Diamonds with predominantly A or B defects are termed *IaA* and *IaB*. The majority of natural stones belongs to a mixed type *IaAB* or simply *Ia*.

Type *Ia* diamonds, containing nitrogen mainly in aggregated forms, also show a specific type of extended defect called platelets. They are considered as {001} planar structures with a size varying between tens of nanometers and a few micrometers. The first X-ray diffraction (XRD) observations associated with these defects were discovered in 1940 (Raman & Nilakantan, 1940; Lonsdale, 1942). Among various diffuse

features there are diffuse streaks propagating in ⟨001⟩ through Bragg nodes and conserving the periodicity of diamond lattice; these streaks are frequently observed in high-pressure diffraction experiments with diamond–anvil cells. However, there are not many X-ray studies of diffuse scattering in diamonds and they are always limited by the proximity of the Bragg spots (Raman & Nilakantan, 1940; Hoerni & Wooster, 1955; Maeta *et al.*, 2006; Moore *et al.*, 1999; Frank, 1956). Diffuse streaks in reciprocal space correspond to planar objects in real space; the concept of {001} planar structures, platelets, has also been confirmed by the direct TEM and high-resolution TEM (HRTEM) observations [Evans & Phaal, 1962; Barry *et al.*, 1985; Humble, Mackenzie & Olsen, 1985 (I); Humble, Lynch & Olsen, 1985 (II); Fallon *et al.*, 1995]. However, the nature and atomic structure of the platelets remain unknown.

All together, the experimental data collected so far for *Ia* diamonds can be summarized as follows:

(i) the diamond single crystal may be considered as a set of blocks with undistorted diamond lattices separated by thin platelet defects;

(ii) the displacement of the diamond blocks, caused by the presence of platelets, varies between $0.33a_0$ and $0.40a_0$, being perpendicular to the plane of the defect, as seen from XRD (Frank, 1956) and HRTEM data [Barry *et al.*, 1985; Humble, Mackenzie & Olsen, 1985 (I); Humble, Lynch & Olsen, 1985 (II); Fallon *et al.*, 1995];

(iii) the ⟨110⟩ and ⟨1$\bar{1}$0⟩ directions in the platelet plane are non-equivalent (Barry, 1991);

(iv) in some cases a weak periodicity close to $8^{1/2}a_0$ can be seen in the ⟨110⟩ direction (Barry *et al.*, 1985).

The role of nitrogen in the formation of platelets is not yet absolutely clear; the nitrogen content as seen by electron energy-loss spectroscopy (EELS) is consistent within the same diamond but varies from crystal to crystal [Humble, Lynch & Olsen, 1985 (II); Berger & Pennycook, 1982]. The observed nitrogen content corresponds to 0.08–0.47 monolayers [Humble, Lynch & Olsen, 1985 (II)]. This value is too high for a pure carbon interstitial Humble model [Humble, Mackennzie & Olsen, 1985 (I); Humble, Lynch & Olsen, 1985 (II)], but less than required by nitrogen platelet models (Barry, 1991; Lang, 1964); the latter suggests that two monolayers are present. A randomized version of Humble's model with antiphase domain boundaries has also been proposed in order to incorporate the variable nitrogen concentrations (Fallon *et al.*, 1995). Annealing of *Ia* diamond at temperatures in excess of 2673 K under stabilizing pressure converts the platelets to dislocation loops and to the voidites associated with the loops (Evans *et al.*, 1995).

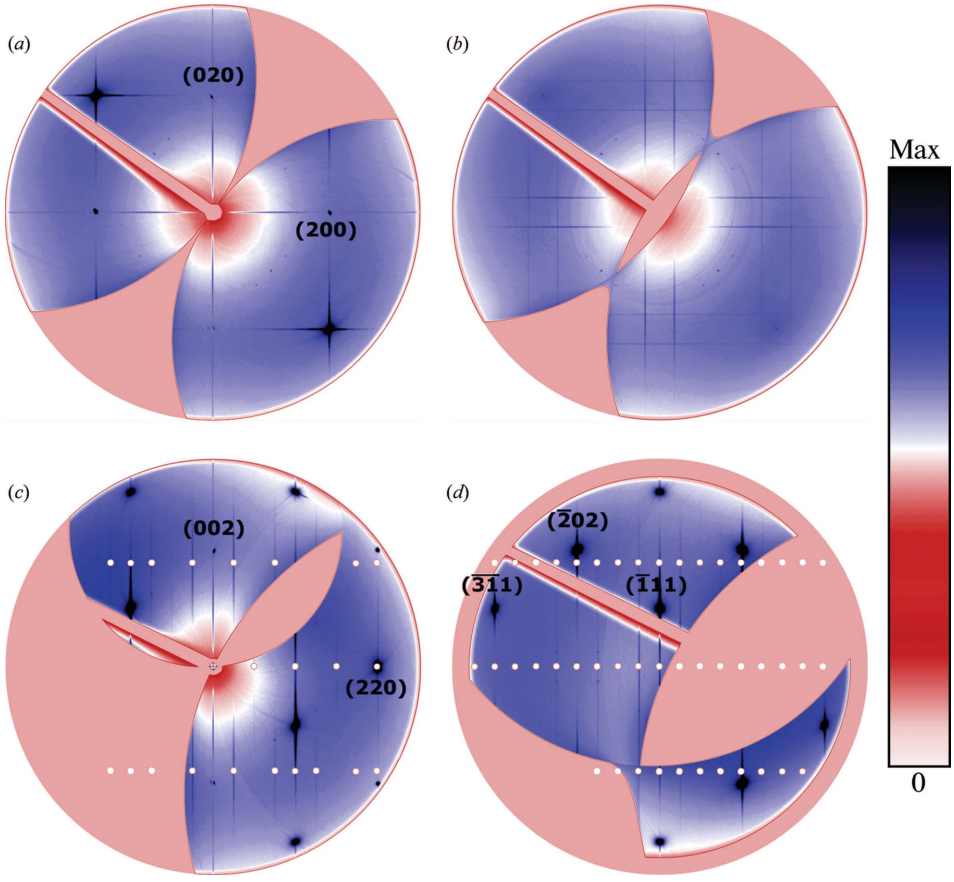

Figure 1
Reciprocal space reconstructions for *Ia* diamond: (*a*) *H K* 0 plane; (*b*) *H K* 1/4 plane; (*c*) *H H L* plane; (*d*) $H-1$ $H+1$ *L* plane. In panels (*c*) and (*d*) model patterns are represented by white points. Note the difference in intensity distribution between Huang scattering emerging from strong Bragg reflections (panel *a*) and diffuse rods do not crossing Bragg nodes (panel *b*).

Few attempts to model the structure of platelets by *ab initio* methods have been undertaken (Goss *et al.*, 2003; Miranda *et al.*, 2004; Goss *et al.*, 2006) and apparently sp^3-bonded self-interstitial models fit better with some experimental data (Goss *et al.*, 2003, 2006). However, due to the quite moderate quantity of available experimental parameters, mostly due to the radiation damage for HRTEM that affects platelet structure (Barry, 1991), the real structure of platelets remains unknown.

In this work we present new diffuse scattering data collected with the help of synchrotron radiation within an extended region of reciprocal space. Every image recorded by an area detector for a given orientation

of crystal and detector is a projection of part of the Ewald sphere on the detector plane. A set of closely spaced projections allows us to reconstruct the desired three-dimensional region of reciprocal space. Such mapping of reciprocal space has actively been used to measure weak diffraction features (see for example Welberry & Butler, 1994), but was never applied for studying diffuse scattering in diamonds. However, diffuse scattering data alone, without modelling, cannot directly uncover the structure of the platelet. We believe that our observations together with concomitant symmetry analysis could provide a solid basis for the theoretical calculations with the crystallographic information reported. From a practical point of view, our observations provide the explanation of data artefacts commonly found for the diamond–anvil cell diffraction experiments.

2. Experiment

In the present study we used diamond–anvil crystals (Almax, geological origin is unknown) not employed previously for high-pressure experiments. In total, three diamonds were tested and the *Ia* class was confirmed by measuring IR absorption spectra, which demonstrate characteristic bands associated with nitrogen complexes and the so-called B′ platelet peak at ~ 1367 cm^{-1}. XRD patterns were recorded at the Swiss–Norwegian Beam Lines (SNBL) of ESRF operating at the bending magnet with wavelength $\lambda = 0.700$ Å in transmission geometry using a MAR345 image-plate detector; the beam was slit down to 0.5×0.5 mm. An angular range of 100° was covered with 0.5° steps in the scanning mode with a typical exposure time of 15 s. The wavelength, scanning range and beam size were chosen to be close to conditions of a high-pressure experiment with a diamond–anvil cell. Reciprocal space reconstructions were prepared using *CrysAlis* software (Oxford Diffraction Ltd, 2008).

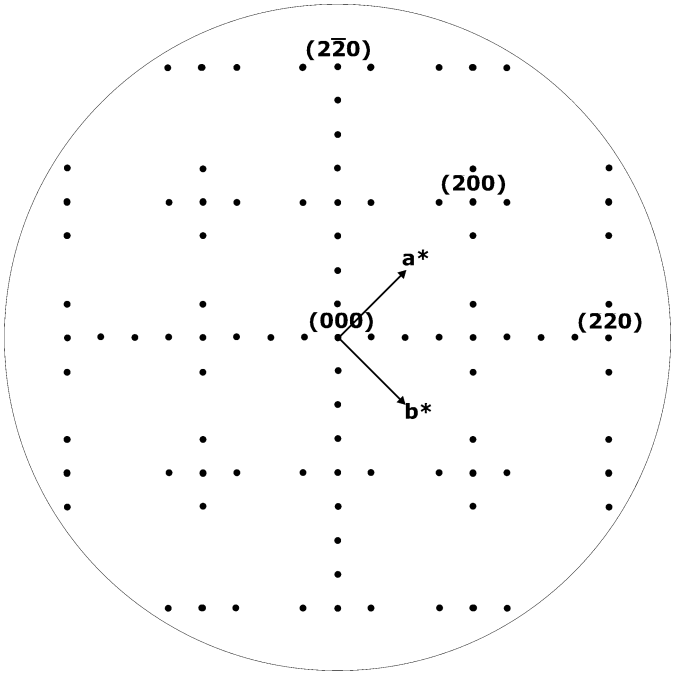

Figure 2
The scheme of ⟨001⟩ diffuse rods network; only those with observable intensity are shown.

3. Results and discussion

The reconstruction of reciprocal space immediately revealed a regular network of orthogonal families of diffuse rods extending through the entire Brillouin zone (see Fig. 1); the picture obtained contains numerous features not identified previously in the XRD data. The diffuse scattering we treat here can be split into three components. First, thermal diffuse scattering (TDS) on long-wavelength acoustic phonons forms smooth-shaped spots around the Bragg positions. This TDS component is superposed with the second component – sharp diffuse streaks propagating in ⟨100⟩ through the Bragg nodes and rapidly decreasing as expected for Huang scattering. We relate this rapidly changing component of diffuse intensity to ⟨100⟩-directed elastic strain in the bulk diamond.

The remaining part of the diffuse scattering consists of rods with the intensity slowly varying along the axis. Such a modulation is related to the structure factor of a platelet itself. The scheme of one out of three orthogonal families of diffuse rods is represented in Fig. 2, where any observable intensity along the corresponding rod is denoted by a solid dot. Periodicity with a $8^{1/2}a_0$ translation is immediately seen along the ⟨110⟩ direction, thus coinciding with occasional HRTEM observations.

Taking into account the non-equivalence of ⟨110⟩ and ⟨1$\bar{1}$0⟩ directions, and the absence of diffuse features at $HK\zeta$ ($H + K = 2n + 1$, ζ propagates along c^*), we conclude that the translation motif within the platelet is $8^{1/2}a_0 \times (1/2)^{1/2}a_0$. Fig. 2 therefore corresponds to a superposition of two twin components related by [010/100/00−1] twinning law. The full three-dimensional pattern of diffuse rods can be described as a superposition of six domains (twins) with *a priori* equal occupancies to keep the average symmetry cubic.

The platelet unit-cell dimension of $\sim 0.55a_0$ can be reconciled with the TEM-derived value of 0.3–$0.4a_0$ if we combine the insertion of a platelet with a symmetry operation leaving the diamond structure undistorted, ($\langle 1/4\ 1/4\ 0\rangle + \langle 0\ 0\ 0.55\rangle \simeq \langle 0\ 0\ 0.3\rangle + \langle 1/4\ 1/4\ 1/4\rangle$; note that $\langle 1/4\ 1/4\ 1/4\rangle$ is a proper translation of the diamond lattice). Moreover, such a translation breaks the tetragonal symmetry of the diamond–diamond interface, making it compatible with the observed rectangular symmetry of platelets. The alternating diffraction patterns along ⟨110⟩ in the (HHL) plane with decreasing intensity for odd rods at $\zeta = 0$ (Fig. 1*c*), and the absence of such alternation along the same direction in the ($H - 1\ H + 1\ L$) plane, indicate that regular absences are due to an open symmetry element (screw axis and/or glide planes), and not to cell centering. The lowest-symmetry space groups in the corresponding Laue classes are orthorhombic $Pmmn$ ($0.55a_0 \times 8^{1/2}a_0 \times (1/2)^{1/2}a_0$) and $Pmn2_1$ ($0.55a_0 \times (1/2)^{1/2}a_0 \times 8^{1/2}a_0$). Model patterns not taking into account the relative intensities are superposed with the

experimental images in Figs. 1(*c*) and (*d*). Determination of lattice spacing along the platelet normal is only an approximant owing to the fact that each platelet diffraction spot is replaced by the Fourier transform of the platelet envelope, which is particularly broad in its normal direction. The decreasing intensity for odd rods with $\zeta = 0$ indicates that the thickness of the platelet object is equal to its lattice spacing in the normal direction.

4. Conclusions

In agreement with previous experimental findings on planar {001} defects, we have refined and extended the geometrical model of structured platelets in diamond. We show here, by measuring diffuse scattering from the *Ia* type diamond, that the translational symmetry of a platelet is $0.55a_0 \times 8^{1/2}a_0 \times (1/2)^{1/2}a_0$, where the short axis corresponds to an approximant for a pseudo-two-dimensional object with $\sim 0.55a_0$ thickness. Taking $0.55a_0$ as a regular translation normal to the platelet would result in a structure whose highest symmetry corresponds to one of two space groups, *Pmmn* or $Pmn2_1$ [the latter assumes permutated translations $0.55a_0 \times (1/2)^{1/2}a_0 \times 8^{1/2}a_0$]. This symmetry information together with observed diffuse scattering patterns could be used to evaluate the predictive power of theoretical models. Additionally, our data drove us to the conclusion that the diamond blocks, joined by the platelet, are also shifted relative to each other by the $\langle 1/4\ 1/4\ 0 \rangle$ translation.

We would like to underline a few outcomes of this work. First, it has been reported that the formation of platelet defects can be induced in the laboratory by annealing *IaA*-type diamonds at temperatures over 2773 K (Kiflawi *et al.*, 1998). These 'man-made' platelets exhibit IR absorption spectra which are slightly different from those of 'normal' platelets in *Ia* diamonds; unfortunately, the diffuse scattering data are not available. If established, the correlation between pressure–temperature history of diamond and its diffuse scattering pattern will potentially help to reveal the geophysical processes recorded in diamond defect structure. The second aspect concerns the diamond–anvil cell (DAC) technique, as *Ia* diamonds are indeed the most frequently used anvils. Typically the diffraction patterns recorded in DACs are contaminated by parasitic diffuse scattering, which manifests itself as more or less a random set of sharp spots and/or lines. This scattering is of elastic nature and corresponds to a section of platelet-related diffuse rods by an Ewald sphere. This contribution to the scattering patterns is generally not welcome and may compromise the quality of both elastic and inelastic scattering experiments. As the diffuse scattering is now rationalized as a pattern with known symmetry, planning of artefact-free experiments or efficient *a posteriori* masking can be applied.

References

Barry, J. C. (1991). *Philos. Mag. A*, **64**, 111–135.
Barry, J. C., Bursill, L. A. & Hutchison, J. L. (1985). *Philos. Mag. A*, **51**, 15–49.
Berger, S. D. & Pennycook, S. J. (1982). *Nature*, **298**, 635–637.
Davies, A. R., Field, J. E., Takahashi, K. & Hada, K. (2004). *J. Mater. Sci.* **39**, 1571–1574.
Evans, T., Kiflawi, I., Luyten, W., van Tendeloo, G. & Woods, G. S. (1995). *Proc. R. Soc. London Ser. A*, **449**, 295–313.
Evans, T. & Phaal, C. (1962). *Proc. R. Soc. London Ser. A*, **270**, 538–552.
Fallon, P. J., Brown, L. M., Barry, J. C. & Bruley, J. (1995). *J. Philos. Mag. A*, **72**, 21–37.
Frank, F. C. (1956). *Proc. R. Soc. London Ser. A*, **237**, 168–174.
Goss, J. P., Briddon, P. R., Jones, R. & Heggie, M. I. (2006). *Phys. Rev. B*, **73**, 115204-1–115204-6.
Goss, J. P., Coomer, B. J., Jones, R., Fall, C. J., Briddon, P. R. & Öberg, S. (2003). *Phys. Rev. B*, **67**, 165208-1–165208-15.
Hoerni, J. A. & Wooster, W. A. (1955). *Acta Cryst.* **8**, 187–194.
Humble, P., Lynch, D. F. & Olsen, A. (1985). *Philos. Mag. A*, **52**, 623–641.
Humble, P., Mackenzie, J. K. & Olsen, A. (1985). *Philos. Mag. A*, **52**, 605–621.
Kiflawi, I., Bruley, J., Luyten, W. & Antendeloo, G. V. (1998). *Philos. Mag. B*, **78**, 299–314.
Lang, A. R. (1964). *Proc. Phys. Soc.* **84**, 871–876.
Lonsdale, K. (1942). *Proc. R. Soc.* **179**, 315–320.
Maeta, H., Matsumoto, N., Haruna, K., Saotome, T., Ono, F., Sugai, H., Ohtsuka, H. & Ohashi, K. (2006). *Physica B*, **376**, 283–287.
Miranda, C. R., Antonelli, A. & Nunes, R. W. (2004). *Phys. Rev. Lett.* **93**, 265502-1–265502-4.
Moore, M., Golshan, M., Kowalski, G., Reid, J., Collins, S. & Murphy, B. (1999). *J. Phys. D Appl. Phys.* **32**, A37–A41.
Neves, A. J. & Nazaré, M. H. (2001). Editors. *Properties, Growth and Applications of Diamond*. INSPEC. EMIS Group, Institution of Electrical Engineers.
Oxford Diffraction Ltd (2008). *CrysAlis*, Version 1.171.32.29. Oxford Diffraction, Abingdon, Oxfordshire, England.
Raman, C. V. & Nilakantan, P. (1940). *Proc. Ind. Acad. Sci. A*, **11**, 389–397.
Webb, S. W. & Jackson, W. E. (1995). *J. Mater. Res.* **10**, 1700–1709.
Welberry, T. R. & Butler, B. D. (1994). *J. Appl. Cryst.* **27**, 205–231.
Zaitsev, A. M. (2001). *Optical Properties of Diamond.* Berlin: Springer.